Materials Research Proceedings 41 (2024) 264-270 https://doi.org/10.21741/9781644903131-30

Finite element modeling (FEM) as a design tool to produce thin wall structures in laser powder bed fusion (L-PBF)

POLLARA Gaetano[1,a *], PALMERI Dina[1,b], BUFFA Gianluca[1,c] and FRATINI Livan[1,d]

[1]Dipartimento di Ingegneria, Università Degli Studi di Palermo, Viale delle Scienze, Palermo, 90128, Italy

[a]gaetano.pollara@unipa.it, [b]dina.palmeri@unipa.it, [c]gianluca.buffa@unipa.it, [d]livan.fratini@unipa.it

Keywords: Numerical Simulation, Laser Powder Bed Fusion, Ti-6Al-4V

Abstract. Laser Powder Bed Fusion (LPBF) has been widely adopted in many industrial sectors such as biomedical, automotive, and aerospace thanks to the possibility to produce objects with complex shapes and meet customers' needs. Despite all the advantages that LPBF can offer, the rise of residual stress due to the high thermal gradients generated during the process can limit its application. This is the case with thin-wall structures where the build-up of residual stress can compromise the success of the printing process. Being able to print this structure can be useful in fuel cell applications where the implementation of cooling channels in bipolar plates can improve their performance. This paper aims to provide guidelines for designing thin-wall structures produced by LPBF processes through numerical simulations by understanding the effect of residual stress on part distortion.

Introduction

Nowadays, where the energy demand is constantly increasing and fossil-based fuels are the principal contributors to meeting the global energy need, hydrogen-based technologies can offer a good alternative to non-renewable energy sources that are doomed to be exhausted one day. Moreover, thanks to its inherently immense energy content, availability, and zero-emission, hydrogen is considered the future fuel in the transport sector. Particularly, hydrogen can be used in electrical power generation systems such as fuel cells for vehicles [1]. These kinds of fuel cells which use chemical hydrogen bonds to store electricity are known as proton exchange membrane (PEM) fuel cells. Bipolar plates (BSs) are the main component of PEM fuel cells in terms of structural strength, weight, and cost [2]. Usually, BPs are made of graphite because of its high conductivity, high corrosion resistance, low density, and ease of fabrication. However, manufacturing of graphite plates under a certain thickness can be difficult due to their brittle nature. Furthermore, it is very challenging to create flow channels in order to apply liquid cooling and improve the PEM fuel cells' performance [3]. As a consequence, metallic plates are taking increasing interest due to their high thermal and electrical conductivity, good gas impermeability, high strength, and good formability. In addition, by using metals as the material to produce metallic plates, additive manufacturing (AM) methods can be adopted [4]. AM consists of a layer-by-layer production fashion in which the part is obtained by adding layers of material. Thus, allowing the fabrication of parts with a very complex shape or structure. In the case of metallic parts, laser powder bed fusion (L-PBF) is among the more suitable AM technologies. In L-PBF a powder bed is deposited on a build plate within a chamber filled with an inert gas and the metallic powder is selectively melted with a laser heat source according to the slicing file [5].

Titanium alloys can be used to produce metallic plates thanks to their high mechanical strength, high corrosion resistance, and lightweight [6,7]. In this study, Ti-6Al-4V was used in the L-PBF process to print bipolar plates. These BPs are characterized by thin-wall structures which can be

difficult to print due to the rise of residual stress during the L-PBF process that can result in part distortion [8,9]. Numerical simulations can be a useful tool to predict part distortion and avoid job failure. Furthermore, compensation strategies can be adopted based on the results from the numerical simulation. In order to simulate the L-PBF process of large parts, a layer-by-layer approach is necessary to reduce the computational cost [10]. In this paper, a finite element method (FEM) is used to simulate the fabrication of a thin-walled structure through the L-PBF process of Ti-6Al-4V powder. The Bipolar Plate geometry was printed and acquired in order to validate the numerical model. An acquisition method based on the fringe projection approach was employed to obtain the actual geometries of the produced part. The aim is to understand the development of residual stress during the process and its effect on part distortion. Moreover, the influence of the number of real layers in the computational one was evaluated in terms of model accuracy and time efficiency.

FEM model and printing process

Simulation Set-Up. Numerical simulations were carried out to understand the influence of residual stress on the deformation mechanism of thin-wall structures for fuel cell application fabricated with L-PBF. To this aim, the FEM commercial software DEFORM-3D™ v12.0 (V12.0, SFC, Columbus, OH, USA) was used. Because of the large dimensions of the bipolar plates being analyzed (144 x 2 x 114 mm^3), a layer-by-layer approach was adopted. With this method, the whole layer is heated simultaneously during the time step. The element activation is strictly correlated on the used voxel mesh according to the born-dead-elements technique. In this way, by the means of a searching algorithm, the elements within the voxel mesh that are influenced by the heat source are activated. The elements not affected by the power input will not be activated and will not have any role in the computational analysis. For more details about the element activation mode and the use of the voxel mesh refer to [11]. The thin-wall structure designed with Autodesk Fusion 360 was simulated on a base plate of 160 x 160 x 25 mm^3 (Fig. 1) with which sticking conditions were applied to avoid detachment during the simulation of the L-PBF process.

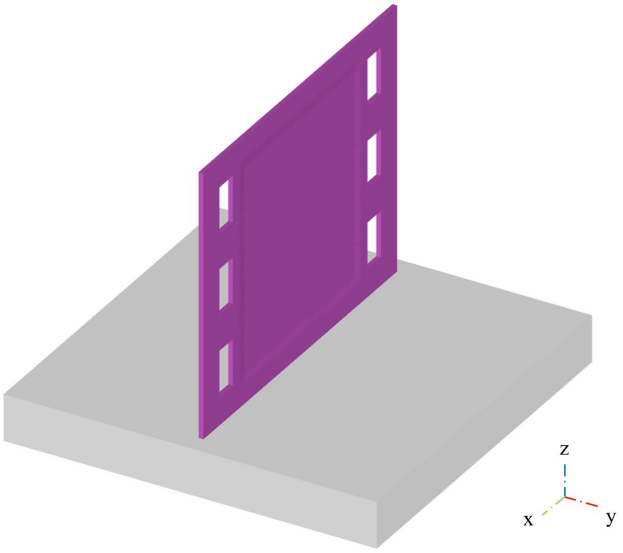

Fig. 1 Thin-wall structure and base plate used for the simulation of the L-PBF process with DEFORM-3D™ v12.0.

In this study, two different voxel meshes were compared named V1 (0.5 x 0.5 x 0.3 mm^3) and V2 (0.5 x 0.5 x 0.6 mm^3) to find the best compromise between simulation accuracy and simulation time. In this way, in the V1 mesh 10 real layers were grouped in one computational layer, while for the V2 mesh, 20 real layers were included in one computational layer. The bipolar plate mesh

consists of 709760 tetrahedral elements and was considered elastoplastic for thermomechanical analysis. For the base plate, instead, 32000 tetrahedral elements were used and the object was modeled as rigid. Ti-6Al-4V was assigned for both the bipolar plate and the build platform as the material. Heat exchange boundary conditions with the environment were defined for both objects by considering the build chamber at 40°C and filled with argon (h_{conv} = 1 W/m^2 °C). To reduce the computational cost and simplify the model, the heat exchange with the powder bed was not taken into consideration. Moreover, the initial built platform temperature was set at 200°C. In order to solve the thermomechanical problem, a Newton-Rapson iteration method was used within DEFORM-3D™ v12.0 using a MUMPS (MUltifrontal Massively Parallel Sparse) solver and a 12th Gen Intel (R) Core (TM) i9-12900 2.40 GHz processor.

Experimental Details. The bipolar plate was fabricated with a 3D system SLM 280 HL machine (SLM Solutions, Lubecca, Germany) to confirm the results from the numerical simulation. A laser power input P equal to 350 W was used together with a scan speed (v) of 1400 mm/s, a hatch spacing (h) equal to 120 µm, and a layer thickness (t) of 30 µm. The platform was preheated to 200°C to reduce the amount of residual stress and the build chamber was filled with argon to lower the oxygen level below 0.1%. In this study, Ti-6Al-4V powder with a Gaussian size distribution of 20-63 µm and spherical shape were used in the L-PBF process.

The printed BP part was removed from the platform and a 3D COMET V system (Steinbichler, Germany) was used to acquire the geometry of the sample. The fringe projection approach is the basis for this 3D acquisition method, where a structured light pattern is projected onto the surface of the object using a projection unit. The image acquisition unit captures the image of the fringe pattern. To measure the component shape at different rotation angles, the printed specimen is placed on a rotating table during the 3D scanning procedure. A three-dimensional representation of the part is created by combining and meshing the point-cloud data sets. Quantifying the distortion of the part was achieved by using the difference in the y-axis (Dy) between the original CAD model and the geometry acquired after the printing process as represented in Fig. 2.

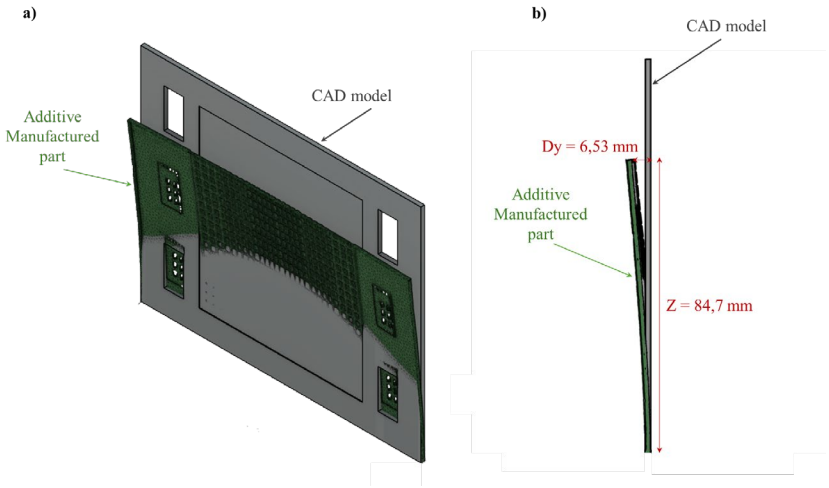

Fig. 2 Comparison between the CAD model of the bipolar plate and the 3D scanned AM part a) 3D view and b) side view with the distortion measurement along the y direction.

Results and discussions

Producing thin-wall structures with L-PBF is still a challenge, especially when large parts are considered as in the case of bipolar plates. The development of residual stresses during the printing process was highlighted as a key factor when creating the BP geometry using additive manufacturing. Significant in-process distortion (as shown in Fig. 3) caused the printing process to end prematurely for a z value of 84.7 mm, corresponding to layer 2851. In detail, a distortion

value of 6.53 mm was observed. In the simulated process, although the level of distortion of the sample is evaluated with a reduced percentage of error, the process does not stop during the creation of the 2851 layer as the development of the distortions, connected to the residual stresses, occurs only following the cooling down phase. This is due to the grouping of several real layers in the computational one and the neglecting of the resting time between consecutive layers. In fact, without considering the interlayer resting time there is no time for the residual stress to develop during the simulation of the process. On the other hand, considering the interlayer resting time results in a significant increase in the simulation time.

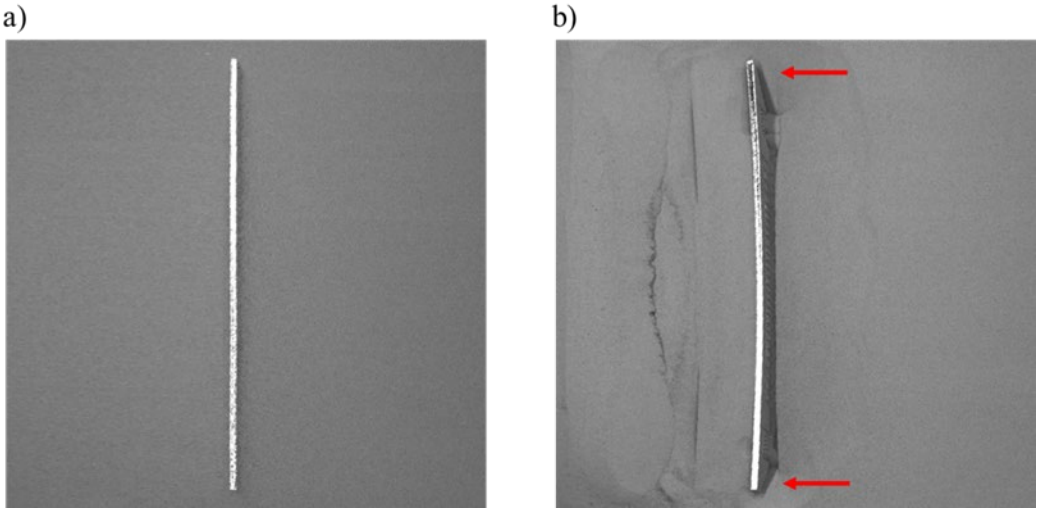

Fig. 3 Post-exposure images acquired during the printing process for a) layer 2850 and b) layer 2851, red arrows indicate the distortion of the part. These images represent the cross-section of the bipolar plate (plane XY), perpendicular to the build direction.

In Fig. 4 it is possible to observe the temperature profiles obtained from the numerical simulation at the end of the printing process.

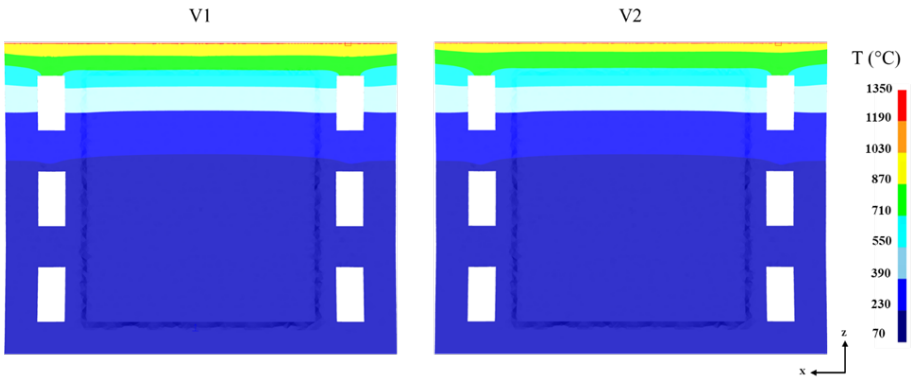

Fig. 4 Temperature profiles for V1 and V2 from the numerical simulation at the end of the printing process.

It can be noted how the temperature profile, in the case of a voxel mesh dimension of 0.3 mm along the z direction (V1), is similar to the one obtained for a voxel mesh dimension of 0.6 mm (V2). A significant difference between the V1 and V2 temperature profiles appears only in the upper part of the component where the temperature is above 700 °C.
Particularly, it can be noted how a finer voxel mesh (V1) better represents the temperature distribution along the z-direction for the last scanned layers with higher temperatures.

The thermal gradient along the z-direction is responsible for the development of the residual stress that can be observed in the numerical simulation after the cooling phase.

In Fig. 5 the residual stresses, for the V1 and V2 cases, developed in the z-direction are shown.

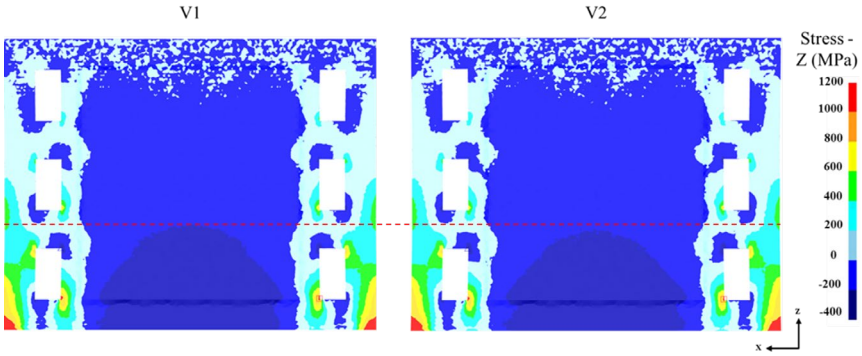

Fig. 5 Residual stress profiles along the z-direction for V1 and V2 obtained from the numerical simulation before the part deformation. The dashed red line highlites the difference in the maximum compression region between V1 and V2.

These stresses caused a large displacement along the y-direction (Fig. 6).

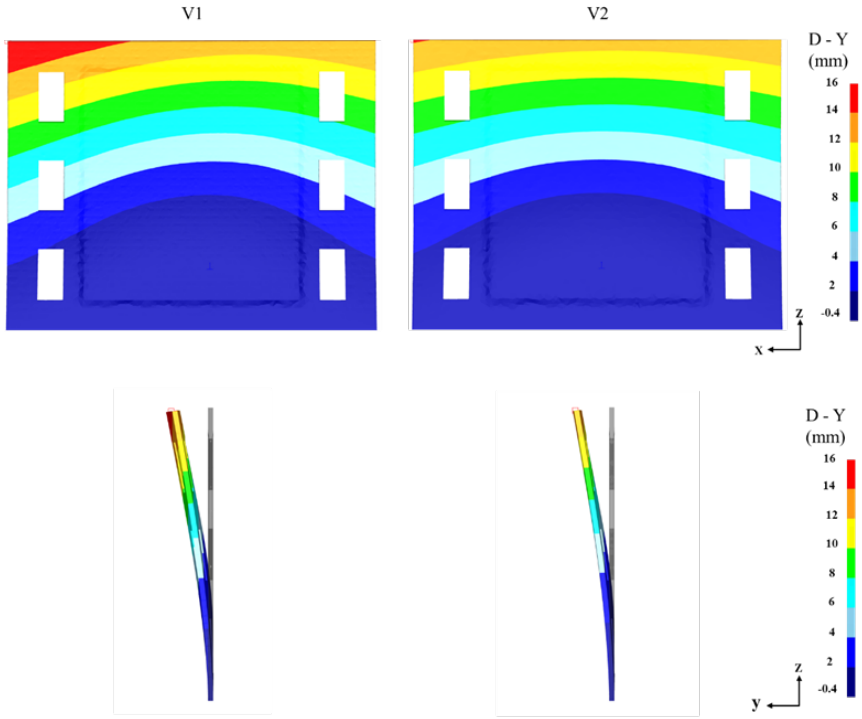

Fig. 6 Displacement profiles along the y-direction for V1 and V2 obtained from the numerical simulation in the ZX and ZY planes.

It can be noted that the V1 case study shows a larger area of maximum compression stress with respect to the V2 case as highlited by the dashed red line. Overall, the V1 voxel mesh allows a better representation of the temperature and residual stress profiles. As a consequence, the displacement from the numerical simulation for the V1 case is closer to the one obtained from the experimental measurement with respect to the V2 case. Also, as can be seen from the displacement maps in the ZX plane, the distribution of the displacement along the y-direction (Dy) is not symmetrical. Moreover, regarding the y displacements, the V1 voxel mesh offers a better match with the real acquired geometry. The difference between the simulated y-displacement and the actual one was evaluated by considering the Dy value at the z = 85.5 mm, which corresponds to the z coordinate of the last printed layer before the premature end of the printing process. As

reported in Fig. 1, this point will result in the z coordinate equal to 84.7 mm after the occurred distortion of 6.53 mm. The Dy values obtained for the V1 and V2 cases are reported in Table 1, equal to 6.03 and 5.72 respectively.

Table 2. Output of the numerical model in terms of displacement, accuracy, and simulation time.

	V1	**V2**
Dy [mm]	6.03	5.72
$Err_{(Dy)}$%	**7.6**	12.4
Simulation Time (gg:hh:mm:ss)	02:07:39:52 (200392 s)	00:20:44:25 (74665 s)
Time Reduction [%]	53.6	**82.7**

Moreover, the accuracy of the simulation model was expressed in terms of percentage error ($Err_{(Dy)}$%) between the Dy measured and simulated at z = 85.5 mm. As shown in Table 1, an $Err_{(Dy)}$% value of 7.6 was found for the V1 voxel mesh and 12.4 for the V2 one. A further analysis regarding the simulation times to simulate the entire process was carried out. In detail, the simulation time was compared to the real printing time introducing a time reduction factor. This factor was calculated as the percentage difference between the printed time and the simulation time of the L-PBF process, by considering a printing time of 432000 s. The V1 voxel mesh resulted in a simulation time of 200392 s and a time reduction of 53.6%, while the V2 resulted in a simulation time of 74665 s and a time reduction of 82.7%. It can be observed how the simulation time is significantly reduced by using a voxel mesh dimension of 0.6 mm (V2) including 20 real layers in one computational layer. The considerable time reduction obtained by using half of the V1 voxel mesh dimension results in one eight of V1 voxel mesh elements. The reduction of the computational time is at the expense of the accuracy of the model as can be seen in Table 1.

Conclusions

In this study, the simulation of the L-PBF process to produce a large Ti-6Al-4V Bipolar Plate was carried out. The influence of the residual stress on the distortion of this thin-walled structure was evaluated together with the accuracy of the numerical model. The main findings of this study are the following:

- Due to the significant development of the residual stresses along the z-direction is not possible to print a Bipolar Plate of the dimension used in this study without any further strategy.
- Even if it is not possible to reproduce exactly when the printing process will end prematurely, the reported displacement from the numerical simulation after the cooling time is very close to the real ones.
- The number of real printed layers included in the computational one has a big impact on the numerical model results both in terms of accuracy and simulation time. In detail, the V1 voxel mesh with 10 real printed layers in one computational layer leads to a better fit with the experimental results. The V2 voxel mesh with 20 real layers in one computational layer, instead, leads to a greater simulation time reduction.
- The good compromise obtained from the numerical model in the case of V1 voxel mesh makes this model a suitable tool for helping engineers in the design of the L-PBF process.

Acknowledgment
Part of this research was funded by Regione Sicilia under the scheme "Azione 1.2.1_03 del PO FESR SICILIA 2014-2020" – Progetto PON03 PE_00206_1 AMELIE ''Advanced framework for Manufacturing Engineering and Product Lifecycle Enhancement.'' CUP G76I20000060007.

References

[1] M.K. Singla, P. Nijhawan, A.S. Oberoi, Hydrogen fuel and fuel cell technology for cleaner future: a review, Environmental Science and Pollution Research 28 (2021) 15607–15626. https://doi.org/10.1007/s11356-020-12231-8

[2] S. Karimi, N. Fraser, B. Roberts, F.R. Foulkes, A review of metallic bipolar plates for proton exchange membrane fuel cells: Materials and fabrication methods, Advances in Materials Science and Engineering 2012 (2012). https://doi.org/10.1155/2012/828070

[3] B.G. Pollet, S.S. Kocha, I. Staffell, Current status of automotive fuel cells for sustainable transport, Curr Opin Electrochem 16 (2019) 90–95. https://doi.org/10.1016/j.coelec.2019.04.021

[4] S. Celik, B. Timurkutluk, U. Aydin, M. Yagiz, Development of titanium bipolar plates fabricated by additive manufacturing for PEM fuel cells in electric vehicles, Int J Hydrogen Energy 47 (2022) 37956–37966. https://doi.org/10.1016/j.ijhydene.2022.08.282

[5] T. DebRoy, H.L. Wei, J.S. Zuback, T. Mukherjee, J.W. Elmer, J.O. Milewski, A.M. Beese, A. Wilson-Heid, A. De, W. Zhang, Additive manufacturing of metallic components – Process, structure and properties, Prog Mater Sci 92 (2018) 112–224. https://doi.org/10.1016/j.pmatsci.2017.10.001

[6] S.H. Wang, J. Peng, W.B. Lui, J.S. Zhang, Performance of the gold-plated titanium bipolar plates for the light weight PEM fuel cells, J Power Sources 162 (2006) 486–491. https://doi.org/10.1016/j.jpowsour.2006.06.084

[7] G. Buffa, D. Palmeri, G. Pollara, F. Di Franco, M. Santamaria, L. Fratini, Process parameters and surface treatment effects on the mechanical and corrosion resistance properties of Ti6Al4V components produced by laser powder bed fusion, Progress in Additive Manufacturing (2023). https://doi.org/10.1007/s40964-023-00440-9

[8] C. Chen, Z. Xiao, H. Zhu, X. Zeng, Deformation and control method of thin-walled part during laser powder bed fusion of Ti–6Al–4V alloy, The International Journal of Advanced Manufacturing Technology 110 (2020) 3467–3478. https://doi.org/10.1007/s00170-020-06104-0

[9] G. Buffa, A. Costa, D. Palmeri, G. Pollara, A. Barcellona, L. Fratini, A new control parameter to predict micro-warping-induced job failure in LPBF of TI6AL4V titanium alloy, International Journal of Advanced Manufacturing Technology 126 (2023). https://doi.org/10.1007/s00170-023-11179-6

[10] T. Lee, U. Auyeskhan, N.-H. Kim, D.-H. Kim, Residual Stress and Dimensional Deviation in a Commercially Pure Titanium Thin Bipolar Plate for a Fuel Cell Using Laser Power Bed Fusion, Metals (Basel) 13 (2023) 1840. https://doi.org/10.3390/met13111840

[11] D. Palmeri, G. Pollara, R. Licari, F. Micari, Finite Element Method in L-PBF of Ti-6Al-4V: Influence of Laser Power and Scan Speed on Residual Stress and Part Distortion, Metals (Basel) 13 (2023) 1907. https://doi.org/10.3390/met13111907